J. Inst. Eng. India Ser. A (June 2019) 100(2):241–252
https://doi.org/10.1007/s40030-019-00364-0

ORIGINAL CONTRIBUTION

Analytical Studies on Debonding Behaviour of RC Beams Strengthened with UHPFRC Overlay

Ramachandra Murthy Avadhanam[1] · Aravindan Muralidharan[2] · Ganesh Prakasam[2]

Received: 6 April 2018 / Accepted: 20 January 2019 / Published online: 31 January 2019
© The Institution of Engineers (India) 2019

Abstract The debonding characteristics of ultra-high-performance fibre-reinforced concrete (UHPFRC)-strengthened structures under certain loading conditions have been investigated in this paper. Debonding of UHPFRC-strengthened structures seldom occurs owing to the fact that the tensile strength and the stiffness of UHPFRC are similar to that of the concrete substrate. This work concentrates mainly on the strengthening scheme where UHPFRC is provided in the form of strips at the tension zone of concrete. The studies on the effect of normal and shear stresses at the interface of the beam and UHPFRC strip with load increments are essential to determine the scheme of strengthening. The effect of interfacial shear and normal stresses near the strip end was studied by using the Tounsi model which is a modification of Teng model. A comparative study on the variation of the interfacial shear and normal stresses for the beams retrofitted with UHPFRC strip and other repair materials has been carried out. In the present study, the variation of stresses is investigated at two load levels with one load close to the pre-damage load given to the beam and the other load close to the ultimate load. Analytical studies are carried out to study the debonding behaviour of damaged RC beams strengthened with UHPFRC strips under static and fatigue loading. Parametric studies have also been carried out to determine the optimum configuration of the strips to be bonded to the beams.

✉ Ramachandra Murthy Avadhanam
murthyarc@serc.res.in; murthycsdg@gmail.com

[1] CSIR-Structural Engineering Research Centre, Chennai 600113, India

[2] AcSIR, CSIR-Structural Engineering Research Centre, Chennai 600113, India

Keywords RC beam · Static loading · Debonding · Ultra-high-performance fibre-reinforced concrete · Retrofitting · Fatigue loading

List of Symbols

ε_1, ε_2	Strains at the top and bottom faces of the adhesive
$u_1(x)$, $u_2(x)$	Longitudinal displacements at the base of concrete and top of UHPFRC layer
ε_1^M, ε_2^M	Strain due to bending moments at the concrete and the UHPFRC layer
ε_1^N, ε_2^N	Strain due to the longitudinal forces at the concrete and the UHPFRC layer
M_1, M_2	Bending moments at the concrete and the UHPFRC layer
N_1, N_2	Longitudinal forces at the concrete and the UHPFRC layer
E_1, E_2	Modulus of elasticity of the concrete and the UHPFRC layer
I_1, I_2	Moment of inertia of the concrete and the UHPFRC layer
y_1, y_2	Distances from the bottom of the concrete layer and the top of UHPFRC layer to their respective centroids
u_1^N, u_2^N	Displacement induced by longitudinal force of the respective adherends
σ_p	Axial stress in the plate
σ_c	Axial stress in the concrete prism
τ	Shear stress in the adhesive layer
t_p	Thickness of the plate
t_c	Thickness of the concrete prism
τ_f	Local bond strength
δ	Interfacial slip, relative displacement between the two adherends

b_p, b_c	Width of the plate and the concrete prism
G_f	Interfacial fracture energy
σ_1	Normal stress at the strip
G_c	Interfacial fracture energy
τ_{f0}, τ_{ft}	Cycle-dependent bond strengths at time zero and time t in min
δ_{ft}	Cycle-dependent slip
α	Frequency-dependent factor
P	Load
Z	Length of the softening zone
m, n	Material constants
β	Fatigue debonding growth coefficient

Introduction

Strengthening or retrofitting of the damaged concrete structures due to upgradation of loads and severe environmental condition has been significantly addressed in the last few decades. Reinforced concrete beams which form an integral part of structural system are more prone to the damage during their service lifetime. To address these issues, various strengthening techniques and new repair materials are developed. Most of the repair materials supplemented with suitable strengthening techniques tend to satisfy the criteria for strength restoration or upgradation. But they fail to satisfy the environmental durability criterion resulting in the loss of efficiency of the retrofit system. In addition to predict the debonding behaviour of retrofitted beams under monotonic loading, it is also essential to predict the debonding behaviour under fatigue loading. This becomes significant in situations such as bridges subjected to traffic loads and buildings subjected to wind-induced fatigue.

In a typical strengthening system, the performance of strip–beam interface in providing the means for effective stress transfer is of utmost importance. A number of failure modes in strip-strengthened beams are directly caused by the interfacial debonding between the composite strip of materials and the concrete beam [1–3]. One of the failure modes, referred to as intermediate crack-induced debonding (IC debonding), involves debonding of the composite plate or strip which initiates at a major crack such as flexural or flexure-shear crack and propagates along the strip-to-concrete interface. Debonding is likely to happen at the ends of the strip due to the combination of high normal and shear stresses. Predominantly, failure occurs due to the latter which qualifies for the mode of failure to be referred as Mode II [4–6].

The intermediate crack(IC)-induced debonding may be classified into two types. The first type involves initiation of debonding from a crack in a strip under tension and propagation towards the free end of the strip [7]. The studies reported in the literature reveal that the main failure mode of this type of strengthening system is the concrete failure under shear occurring near the concrete–adhesive interface. The ultimate load that the interface can carry depends predominantly on the concrete strength beyond which a particular value of bond length cannot increase which is termed as the effective bond length.

In normal RC beams bonded with an FRP soffit plate, series of cracks are generally distributed along the length of the beam. As a result, between the major flexural or flexural-shear crack where debonding initiates and the stress-free ends of the plate, causes initiation of other cracks. The mechanics of the debonding process in such beams can be significantly different from that of a simple pull-out test specimen. These failures may be termed as the second type of IC debonding failures to distinguish them from the first type of IC debonding failures.

When it comes to the case of fatigue loading, it was reported in the literature that introduction of composite material in the tension zone of the reinforced concrete beams resulted in significant reduction in longitudinal steel stress and increase in the fatigue life of the beams [8, 9]. But it was also observed that the premature detachment of the composite strips from the concrete substrate again increased the stress range in the reinforcing steel. This can be attributed to the debonding of the strip which redistributes the stress back to the internal steel reinforcement.

The cases of debonding have seldom been reported in the literature regarding ultra-high-performance concrete (UHPC)-strengthened structures. This is due to the fact that the tensile strength and the stiffness of UHPC are more similar to those of the concrete substrate in comparison with the other repair materials such as FRP and steel. There is a need to determine the influence of shear stresses developed at the edge of the strips and between the cracks in a view to determine the optimum bond length and thickness of the strips. Also accurate predictions of interfacial stresses are important for designing guidelines for composite strip-strengthened RC beams against the debonding failures. Some articles reported in the literature have modelled the thick laminated composite plates based on higher-order shear deformation theory [10–12]. However, finite element and analytical studies on the ultimate load failure prediction and modes of failure of the laminated plates have been carried out by the researchers in the recent past [13, 14]. In the present study, the popular models such as Tounsi model (2006), Teng model (2006) and Diab model (2009) are employed to predict the debonding behaviour of retrofitted RC beams under monotonic and fatigue loading [15–17].

Models for Debonding Studies

This section discusses the various analytical models employed in the present study for debonding behaviour of damaged RC beams strengthened with UHPFRC precast strips.

Tounsi Model (2006)

The intermediate crack-induced debonding (first type) was addressed by suggesting a closed-form solution which is an improved method of Teng model [4, 15]. The model reasonably assumes that the shear stress distribution is continuous across the adhesive–adherend interface and the shear stress be zero at the free surface to satisfy the equilibrium. Shear deformation in the adherents is ignored as suggested in the literature [18, 19].

To start with a differential element of size dx is considered from the strengthened beam (Figs. 1, 2). The beam is comprised of three layers of materials namely reinforced concrete, adhesive and UHPFRC.

The basic assumptions made in the formulation are:

- All materials behave in a linear elastic manner.
- The adhesive is responsible only for transferring stresses from one adherend to other.
- The stresses in the adhesive layer remain constant throughout its thickness.

Following the above assumptions, the strains at the top and bottom faces of the adhesive can be expressed as follows:

$$\varepsilon_1(x) = \frac{\mathrm{d}u_1(x)}{\mathrm{d}x} = \varepsilon_1^M(x) + \varepsilon_1^N(x) \tag{1}$$

$$\varepsilon_2(x) = \frac{\mathrm{d}u_2(x)}{\mathrm{d}x} = \varepsilon_2^M(x) + \varepsilon_2^N(x) \tag{2}$$

where $u_1(x)$ and $u_2(x)$ are the longitudinal displacements at the base of concrete and top of UHPFRC layer, respectively. $\varepsilon_1^M(x)$ and $\varepsilon_2^M(x)$ and $\varepsilon_1^N(x)$ and $\varepsilon_2^N(x)$ are the respective strains induced due to bending moments and the longitudinal forces at the concrete and UHPFRC layer, respectively, which are given as follows:

$$\varepsilon_1^M(x) = \frac{M_1(x)y_1}{E_1 I_1};\ \varepsilon_2^M(x) = \frac{-M_2(x)y_2}{E_2 I_2} \tag{3}$$

$$\varepsilon_1^N(x) = \frac{\mathrm{d}u_1^N(x)}{\mathrm{d}x};\ \varepsilon_2^N(x) = \frac{\mathrm{d}u_2^N(x)}{\mathrm{d}x} \tag{4}$$

where y_1 and y_2 are distances from the bottom of the concrete layer and the top of UHPFRC layer to their respective centroids and u_1^N and u_2^N are the longitudinal force-induced displacements of the respective adherends.

Complete details are available in Tounsi model [15].

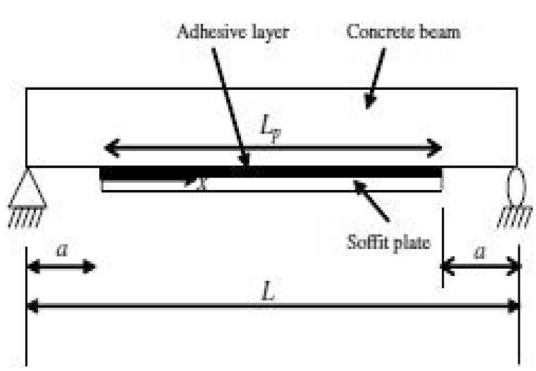

Fig. 1 Simply supported beam strengthened with a composite strip

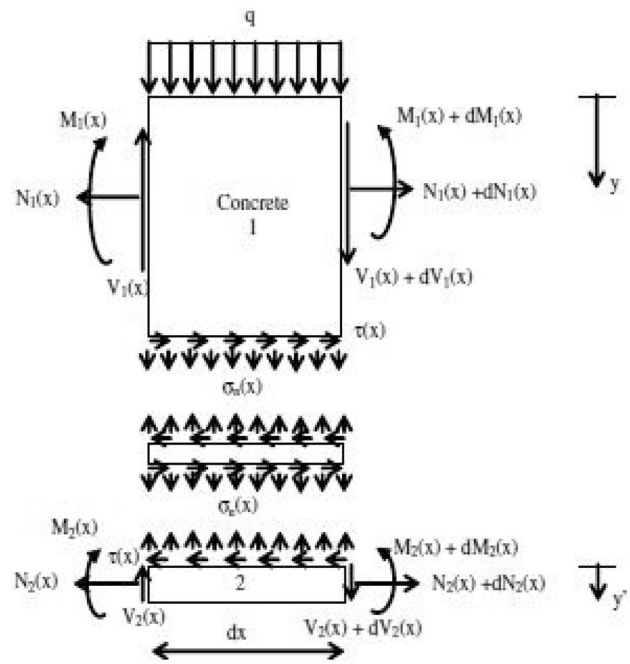

Fig. 2 Forces in an infinitesimal element of a strengthened beam

Teng Model (2006)

The problem of the second type of IC debonding discussed earlier is addressed by making use of a closed-form formulation [16]. This formulation is originally developed to understand the behaviour of FRP-to-concrete interface between two adjacent cracks, but can be extended to problems involving other composite materials. It presents the behaviour of the interface where the composite strip is subjected to different tensile forces at the two ends while the concrete beam or prism is subjected to two different axial forces which may be either compressive or tensile at the two ends as shown in Fig. 3. A bilinear bond–slip model is assumed for the prediction of the debonding process in the model.

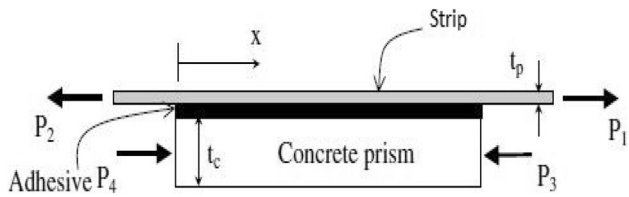

Fig. 3 Idealized model of UHPFRC concrete bonded joint between two adjacent cracks

The model is constructed with the notion of the strip as a plate and beam as a prism. The plate is subjected to two tensile forces P_1 and P_2 at the left and right end, respectively, whereas the concrete prism is subjected to two forces P_3 and P_4 which can be either compressive or tensile.

The basic assumptions considered in this formulation are as follows:

(1) All the forces remain proportional to each other throughout the loading process.
(2) The cross-sectional dimensions of the plate and prism remain constant along the length.
(3) The adhesive layer is of constant thickness, and the whole model is in a plane stress state.

The adhesive layer is thus subjected to shear deformations while the adherents are subjected to axial deformations in the light of the above specified assumptions. So the bending deformation of the adherents is neglected, and the shear stress across the adhesive layer is assumed to be constant.

The equilibrium considerations will result in the following equations based on the above assumptions [20]:

$$\frac{\mathrm{d}\sigma_p}{\mathrm{d}x} - \frac{\tau}{\tau_p} = 0 \tag{5}$$

$$\sigma_p t_p \sigma_p + \sigma_c t_c \sigma_c = P = P_1 - P_3 = P_2 - P_4 \tag{6}$$

where σ_p is the axial stress in the plate, σ_c is the axial stress in the concrete prism, τ is the shear stress in the adhesive layer, t_p is the thickness of the plate and t_c is the thickness of the concrete prism.

The interfacial shear stress can be expressed as a function of interfacial slip (constitutive equation for the adhesive) which is given as follows:

$$\tau = f(\delta) \tag{7}$$

Similarly, the constitutive equations for both the adherents are given as follows:

$$\sigma_p = E_p \frac{\mathrm{d}u_p}{\mathrm{d}x} \tag{8}$$

$$\sigma_c = E_c \frac{\mathrm{d}u_c}{\mathrm{d}x} \tag{9}$$

The interfacial slip δ in Eq. (7) is the relative displacement between the two adherends

$$\delta = u_p - u_c \tag{10}$$

After substituting equations Eqs. (6)–(10) in Eq. (5), we get

$$\frac{\mathrm{d}^2\delta}{\mathrm{d}x^2} - f(\delta)\left(\frac{1}{E_p t_p} + \frac{b_p}{b_c E_c t_c}\right) = 0 \tag{11}$$

and

$$\sigma_p = \frac{\left(\frac{\mathrm{d}\delta}{\mathrm{d}x} + \frac{P}{b_c E_c t_c}\right)}{t_p\left(\frac{1}{E_p t_p} + \frac{b_p}{b_c E_c t_c}\right)} \tag{12}$$

where b_p and b_c are the widths of the plate and the concrete prism, respectively.

Introducing the fracture parameters of local bond strength τ_f and interfacial fracture energy G_f in Eqs. (11) and (12), we get

$$\frac{\mathrm{d}^2\delta}{\mathrm{d}x^2} - \frac{2G_f}{\tau_f^2}\lambda^2 f(\delta) = 0 \tag{13}$$

$$\sigma_p = \frac{\tau_f^2}{2G_f t_p \lambda^2}\left(\frac{1}{E_p t_p} + \frac{b_p}{b_c E_c t_c}\right) \tag{14}$$

where

$$\lambda^2 = \frac{\tau_f^2}{2G_f}\left(\frac{1}{E_p t_p} + \frac{b_p}{b_c E_c t_c}\right) \tag{15}$$

Details related to complete formulation can be found in Teng model [13].

Diab Model (2009)

The evolution of the debonding of FRP strips bonded to the reinforced concrete beams under fatigue loading was studied [17]. The fatigue performance of the FRP–concrete interface is investigated through an analytical procedure by considering the effect of cycles in the bond–slip behaviour. This procedure can also be extended to other composite materials.

The formulation used in this work is an extension of the above-discussed debonding model which can be used for the case of fatigue loading. Similar to the previously discussed models, the adhesive layer in this model is assumed to be subjected to pure shear and the adherents are subjected to pure axial deformation. The thickness and width of the layer are t_1 and b_1 for UHPFRC strip and t_2 and b_2 for the concrete beam, respectively. The bonded length of the strip is taken as L.

The governing differential equations for the slip are governed by the following equations which are same as those of the previous formulation:

$$\frac{d^2\delta}{dx^2} - \frac{2G_c}{\tau_f^2}\lambda^2 f(\delta) = 0 \tag{16}$$

$$\sigma_1 = \frac{\tau_f^2}{2G_c t_1 \lambda^2}\frac{d\delta}{dx} \tag{17}$$

$$\lambda^2 = \frac{\tau_f^2}{2G_c}\left(\frac{1}{E_1 t_1} + \frac{b_1}{b_2 E_2 t_2}\right) \tag{18}$$

where σ_1 is the normal stress at the strip, E_1 and E_2 are the Young's moduli of the strip and beam, respectively, and G_c is the interfacial fracture energy.

As discussed earlier, a bilinear model as shown in Fig. 4 is used for the representation of bond–slip behaviour which has been modified to accommodate the degradation of stiffness and strength of the interface while the fracture energy is kept constant.

The cycle dependence is inducted into the model by introducing creep-fatigue coefficient ϕ obtained from the experiments to represent the degradation of the interfacial stiffness [17]. The cycle-dependent bilinear model is given below:

$$f(x) = \left\{ \begin{array}{ll} \frac{\tau_{ft}}{\delta_1}\delta, & 0 \le \delta \le \delta_1 \\ \frac{\tau_{ft}}{(\delta_{ft} - \delta_1)}(\delta_{ft} - \delta), & \delta_1 \le \delta \le \delta_{ft} \end{array} \right\} \tag{19}$$

where

$$\tau_{ft} = \frac{\tau_{f0}}{1 + \phi.\alpha} \tag{20}$$

$$\phi = \left\{ \begin{array}{ll} 0.046t^{0.4}, & t \le 2000 \\ 1.2(1 - \exp(-t/1200)), & t > 2000 \end{array} \right\} \tag{21}$$

where τ_{f0}, τ_{ft} are cycle-dependent bond strengths at time zero and time t in min, $\delta_{ft} = \tau_{f0}\delta_{t0}/\tau_{ft}$ is the cycle-dependent slip and α is the frequency-dependent factor.

Substituting the above bilinear model in Eq. (16), the following equations are obtained.

$$\frac{d^2\delta}{dx^2} - \lambda_1^2\delta = 0 \quad \text{for } 0 \le \delta \le \delta_1 \tag{22}$$

$$\frac{d^2\delta}{dx^2} + \lambda_2^2\delta = \lambda_2^2\delta_{ft} \quad \text{for } \delta_1 \le \delta \le \delta_{ft} \tag{23}$$

where

$$\lambda_1^2 = \frac{\tau_{ft}}{2G_f}\left(\frac{1}{E_p t_p} + \frac{b_p}{b_c E_c t_c}\right) \tag{24}$$

$$\lambda_2^2 = \frac{\tau_{ft}}{\delta_{ft} - \delta_1}\left(\frac{1}{E_p t_p} + \frac{b_p}{b_c E_c t_c}\right) \tag{25}$$

Using the appropriate boundary conditions [17], the solution of the stress state can be expressed as follows:

For $0 \le \delta \le \delta_1$

$$\delta = \delta_1 \frac{\cosh(\lambda_1 x)}{\cosh[\lambda_1(L - z)]} \tag{26}$$

$$\tau = \tau_{ft}\frac{\cosh(\lambda_1 x)}{\cosh[\lambda_1(L - z)]} \tag{27}$$

$$\sigma_1 = \frac{\tau_{ft}}{t_1\lambda_1}\frac{\sinh(\lambda_1 x)}{\cosh[\lambda_1(L - z)]} \tag{28}$$

For $\delta_1 \le \delta \le \delta_{ft}$

$$\delta = (\delta_{ft} - \delta_1)\left\{\frac{\lambda_2}{\lambda_1}\tanh[\lambda_1(L - z)] \times \sin[\lambda_2(x - L + z)] - \cos[\lambda_2(x - L + z)] + \frac{\delta_{ft}}{(\delta_{ft} - \delta_1)}\right\} \tag{29}$$

$$\tau = -\tau_{ft}\left\{\frac{\lambda_2}{\lambda_1}\tanh[\lambda_1(L - z)] \times \sin[\lambda_2(x - L + z)] - \cos[\lambda_2(x - L + z)]\right\} \tag{30}$$

$$\sigma_1 = \frac{\tau_{ft}}{\lambda_2 t_1}\left\{\frac{\lambda_2}{\lambda_1}\tanh[\lambda_1(L - z)] \times \cos[\lambda_2(x - L + z)] + \sin[\lambda_2(x - L + z)]\right\} \tag{31}$$

where x is the distance from the free end of the strip as shown in Fig. 5 which shows the shear stress distribution due to fatigue crack and z is the length of the softening zone which increases with the increase in load P before the initiation of the macro-debonding.

The softening length z and the load P can be related by the following equation:

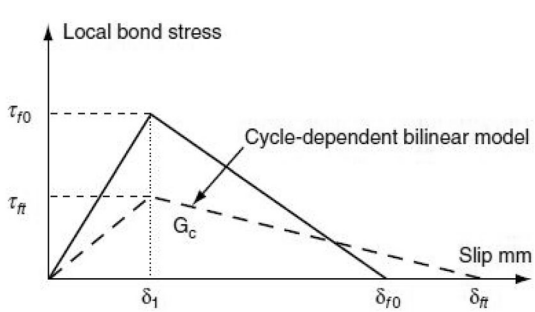

Fig. 4 Cycle-dependent bilinear slip model

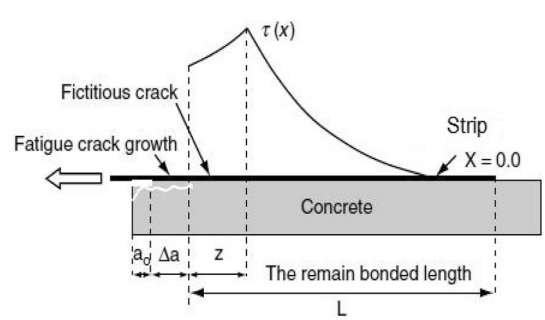

Fig. 5 Shear stress distribution due to fatigue crack

$$P = \frac{\tau_{ft} b_1}{\lambda_2}\left\{\frac{\lambda_2}{\lambda_1}\tanh[\lambda_1(L-z)] \times \cos(\lambda_2 z) + \sin(\lambda_2 z)\right\} \tag{32}$$

The maximum value of P can be obtained from the following equation:

$$P_{\text{max, capacity}} = \frac{\tau_{ft} b_1}{\lambda_2}\left\{\frac{\delta_1}{(\delta_{ft}-\delta_1)}\tan^2 h[\lambda_1(L-z_m)] + 1\right\}\sin(\lambda_2 z_m) \tag{33}$$

where z_m is the maximum length of the softening zone for a given bond–slip curve and can be determined from the following equation through iterative process:

$$\tanh[\lambda_1(L-z_m)] = \frac{\lambda_2}{\lambda_1}\tanh[\lambda_2 z_m] \tag{34}$$

The fracture mechanics-based approach for remaining life prediction assumes that the cycle-fatigue life of the bonded length is dominated by debonding propagation and debonding growth, rather than the initiation of such cracks. Furthermore, ultimate failure occurs when the remaining bonded length of the FRP–concrete interface can no longer sustain the maximum applied load. It is conventional in fracture mechanics to relate rate of debonding per cycle $\mathrm{d}a/\mathrm{d}N$ to the maximum strain energy release rate $G_{\max}$ which can be calculated using the following formula:

$$G_{\max} = \frac{P_{\max}^2}{2b_1^2 E_1 t_1} \tag{35}$$

Since the maximum strain energy release rate depends upon the parameters such as E_1 and t_1 of the strip, the debonding rate can be expressed in relation to the ratio $G_{\max}/G_c$ where G_c is the quasi-static fracture energy.

$$\frac{\mathrm{d}a}{\mathrm{d}N} = m\left(\frac{G_{\max}}{G_c}\right)^n \tag{36}$$

where m and n are material constants.

Experimental results in the literature have shown that the debonding propagation rate decreases significantly with increasing debonding length, a [17]. To consider the effect of the bonding length to the bonding growth, the energy ratio is expressed in terms of the applied load ratio which is given below.

$$\frac{G_{\max}}{G_c} = \frac{P_{\max}^2}{P_{\text{max, capacity}}^2} = \frac{P_{\max}^2}{\left[\left[\frac{\tau_{ft} b_1}{\lambda_2}\left\{\frac{\delta_1}{(\delta_{ft}-\delta_1)}\tan^2 h[\lambda_1(L-z_m)] + 1\right\}\sin(\lambda_2 z_m)\right]\right]^2} \tag{37}$$

It is to be noted that the above equation is not valid for larger bond lengths. Also this model can be construed as a simulation of a concrete prism bonded with strip of smaller bond length subjected to pull-out tests. This model is employed in the present study to predict the behaviour of damaged RC beam strengthened with UHPFRC strip under fatigue loading.

In addition to expressing the energy ratio in terms of applied load ratio, an additional constant called the fatigue debonding growth coefficient β is

$$\frac{\mathrm{d}a}{\mathrm{d}N} = m_1\left(\frac{G_{\max}}{G_c}\right)^{n_1}.\beta \tag{38}$$

From the above equation, the debonded length can be obtained with respect to the number of cycles until the occurrence of total debonding or failure of the specimen.

Results and Discussion

Experimental investigations have already been carried out by the authors for the beams made of normal strength concrete (NSC) strengthened with repair concrete (UHPFRC). Details regarding the mix details and mechanical properties of both NSC and UHPFRC could be referred from the previous work as shown in Table 1 [21, 22]. Tests were conducted for the cases of both static and fatigue loadings. The minimum shear and normal strengths of the UHPFRC mix determined from splitting prism and slant shear tests, respectively, are reported as 11.05 MPa and 3.21 MPa [23]. No cases of debonding were observed during the experimental investigations on strengthened RC beams after failure as shown in Fig. 6. These experimental investigations have been taken as a datum to validate the analytical models studied in the present work. Parametric studies have been carried out for the load values of 60 kN and 80 kN representing the states of the beam post-yielding and prior to failure, respectively. The loads values 60kN and 80kN were based on the earlier experimental studies conducted by the authors [24]. This section discusses the effect of length and thickness of UHPFRC strip on its interfacial shear and normal stresses calculated using Tounsi model [15]. Studies have also been carried out comparing the shear and normal strengths of UHPFRC with those of the conventional retrofit materials such as GFRP and CFRP. This section also discusses the possibility of debonding in UHPFRC-strengthened beams due to the presence of intermediate cracks based on Teng model [16]. The same is extended to the case of fatigue loading as well based on the Diab model [17].

Figures 7 and 8 present the variation of interfacial shear and normal stresses with the distance from the strip end for the retrofit materials UHPFRC, GFRP and CFRP. In this analysis, the Young's moduli of CFRP and GFRP are taken as 140 GPa and 52 GPa, respectively, and shear modulus as 5000 MPa for both the materials [4, 15]. It can be seen

Table 1 Materials, mix proportion and mechanical properties

Concrete	Mix proportion	Curing	Mechanical properties
Normal strength concrete (NSC)	Cement/fine aggregate/coarse aggregate/W/C 1:1.67:1.86:0.45	Water at ambient temperature for 28 days	Comp. Strength = 35 MPa Split tensile strength = 3.2 MPa Fracture energy = 185 N/m Modulus = 30413 MPa
Ultra-high-performance fibre-reinforced concrete (UHPFRC)	Cement/silica fume/quartz sand/quartz powder: W/C 1:0.25:1.1:0.4:0.23 Steel fibres 2% by volume of concrete and the dosage of superplasticizer is 3.5%	Water curing at ambient temperature for 2 days, 200 °C for 1 day. Later water curing till testing.	Comp. Strength = 122.5 MPa Split tensile strength = 20.7 MPa Fracture energy = 13,760 N/m Modulus = 42,978 MPa

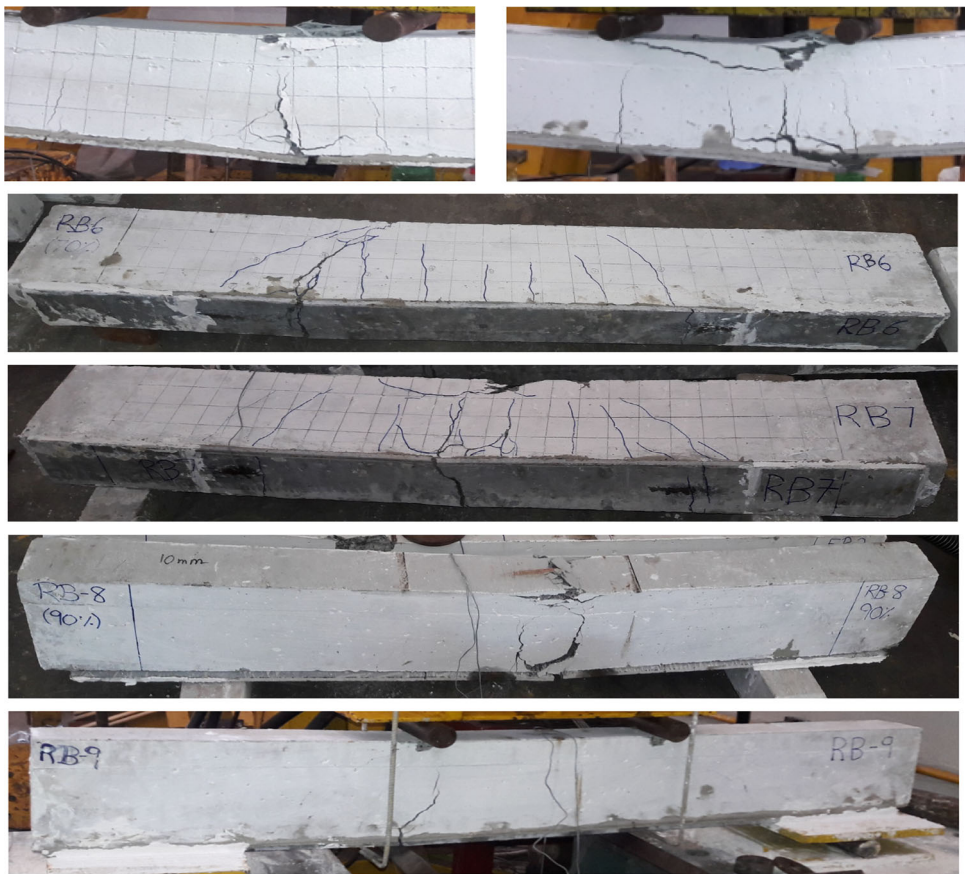

Fig. 6 Typical bonding of UHPFRC on NSC beams after failure

from Figs. 7 and 8 that UHPFRC is found to develop lower values of shear (0.55 MPa) and normal (0.21 MPa) stresses at the interface for a given length and thickness of the strip. It is apparent from these figures that the maximum stresses occur at the free edge of the strip making it a vulnerable location for debonding. But the values of stresses developed in UHPFRC are well within their permissible limits, and hence, the chances of debonding are less as compared to other retrofit materials.

The effect of adhesive thickness (t_a = 2, 3 and 5 mm, respectively) on the interfacial shear stresses is shown in Figs. 9 and 10. Both the interfacial stress distributions are hardly affected by the thickness of the adhesive layer except for the change in their concentration levels. The

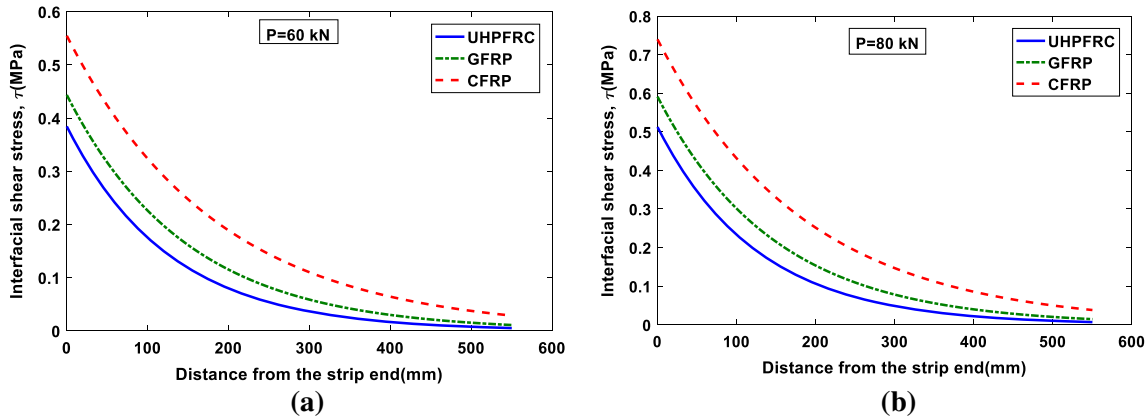

Fig. 7 Effect of strip material on interfacial shear stress at **a** P = 60 kN. **b** P = 80 kN

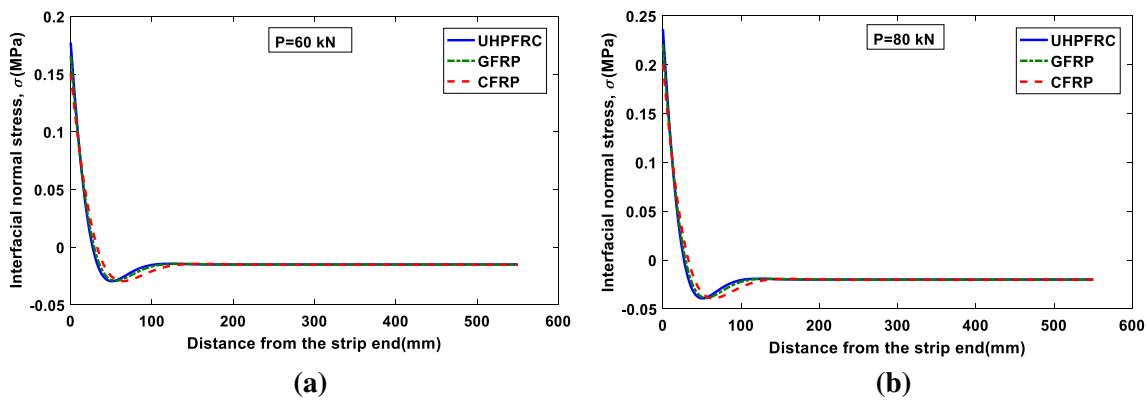

Fig. 8 Effect of strip material on interfacial normal stresses at **a** P = 60 kN. **b** P = 80 kN

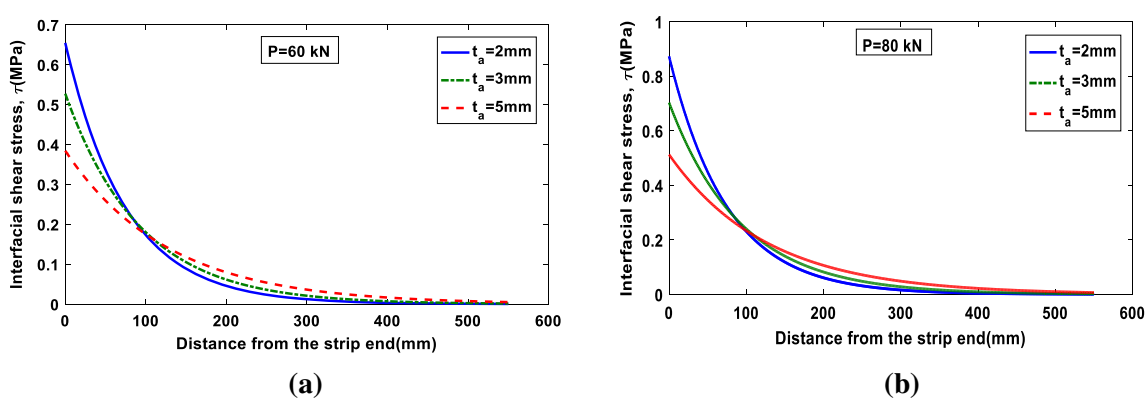

Fig. 9 Effect of adhesive layer thickness on interfacial shear stresses at **a** P = 60 kN. **b** P = 80 kN

effect of the strip thickness (t_s = 5, 8 and 10 mm, respectively) on the interfacial shear stresses is shown in Figs. 11 and 12. The shear stresses are increased, and normal stresses are decreased as a result of increase in the strip thickness. An optimum value of thickness is to be chosen for the strip such that the interfacial stresses are kept well within their limits without compromising on the strength it imparts to the beam to be retrofitted.

Figures 13 and 14 show the effect of length of the strips (L_s = 800, 1000 and 1100 mm, respectively) on the interfacial shear and normal stresses, respectively. The magnitudes of the interfacial stress decrease linearly with the increase in the length of the strips. A bond length equal to the effective length of the beam has been adopted in the experimental investigations for which the interfacial stresses are within the limits of the permissible values. In

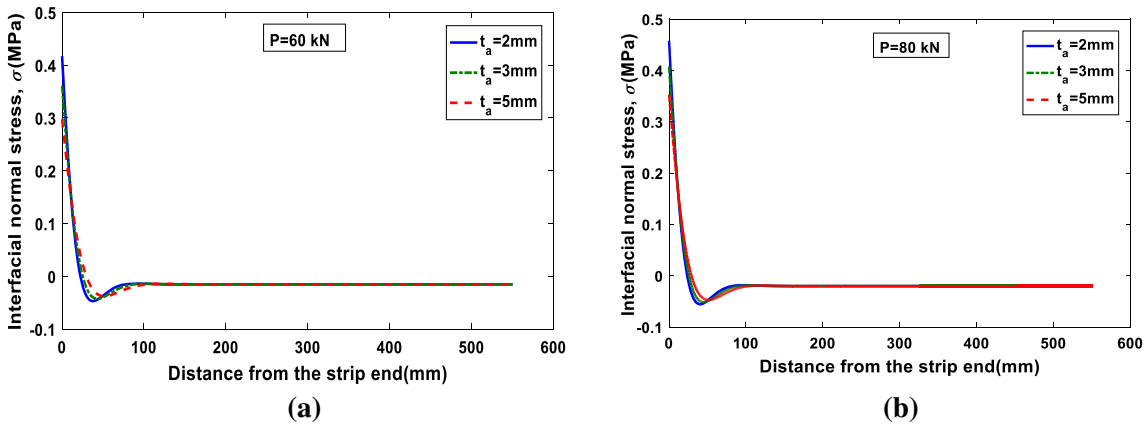

Fig. 10 Effect of adhesive layer thickness on interfacial normal stresses at **a** P = 60 kN. **b** P = 80 kN

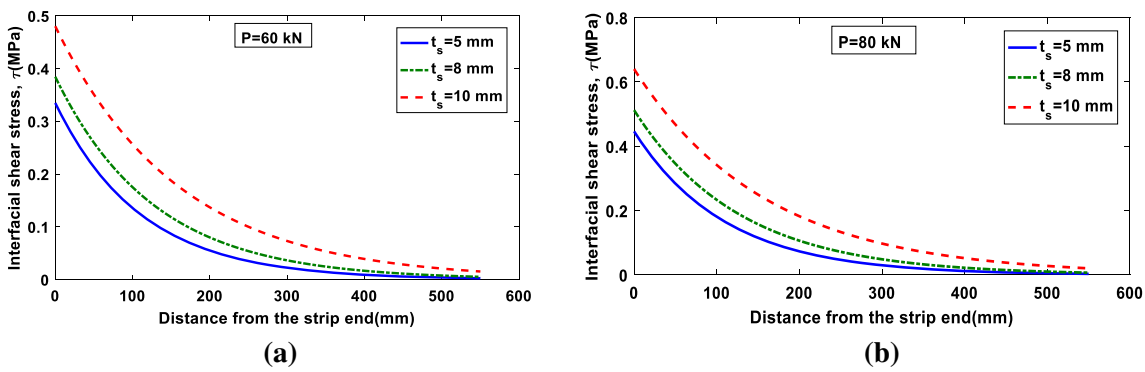

Fig. 11 Effect of strip thickness on interfacial shear stresses at **a** P = 60 kN. **b** P = 80 kN

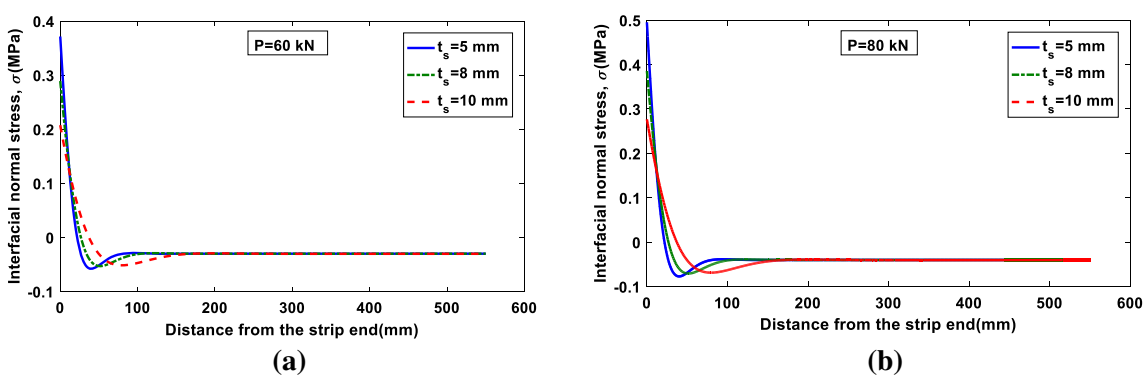

Fig. 12 Effect of strip thickness on interfacial normal stresses at **a** P = 60 kN. **b** P = 80 kN

agreement with the model, for the adopted bond length, no cases of debonding were observed during the experimental investigations.

From all the above parametric studies, it was inferred that the likelihood of debonding initiating at the end of the strip is less for the beams subjected to the load under service conditions.

In the present work, the problem of intermediate crack-induced debonding is restricted to the constant bending moment zone based on Teng model [16].

The values of the parameters adopted in this study are as follows:

$$\beta = \eta = 1,\ \delta_f = 0.34\,\text{mm}, \delta_1 = 0.062\,\text{mm}, \tau_f = 11.05\,\text{MPa}, G_f = 12.03\,N/\text{mm}.$$

A typical bond length of 100 mm representing a typical crack spacing in reinforced concrete beams along with other bond lengths of 10 mm and 20 mm representing closed crack spacing in UHPFRC has been adopted in the

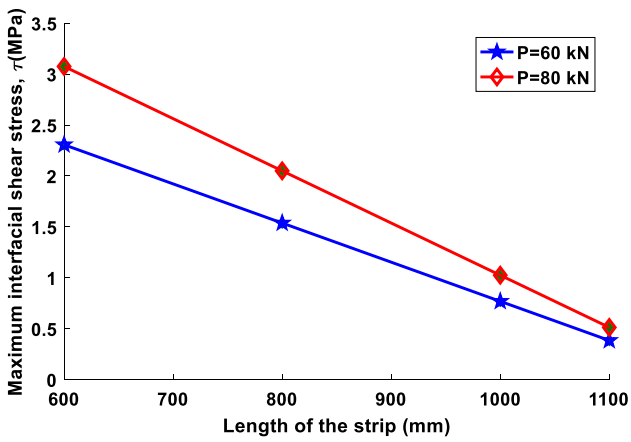

Fig. 13 Effect of length of strip on the interfacial shear stresses

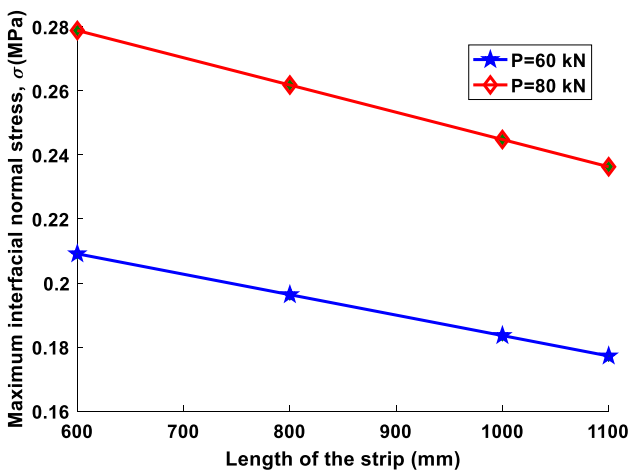

Fig. 14 Effect of length of strip on the interfacial normal stresses

present study [25]. Figure 15 shows the interfacial load–slip behaviour of the strip for various bond lengths.

It can be seen that since $\beta = \eta = 1$, for all three different bond lengths, the interface experiences the same sequence of interfacial shear stress distribution. But the corresponding load–displacement curves are very different in shape. Because both the geometry and the loading are symmetrical, the interfacial shear stress distribution is anti-symmetrical about $x = L/2$. Debonding starts when τ reaches zero at both the ends and then propagates from both the ends towards the middle of the strip which is now in a debonding–softening–elastic–softening–debonding state. As both peak shear stresses τ_f continue to move towards $x = L/2$ from both the sides, the load keeps increasing and the ultimate load becomes infinite if material failure of the strip is not considered. Thus, if the upper bound is taken as the material failure of the plate, it can be obviously inferred at the load corresponding to the material failure, debonding will not occur theoretically.

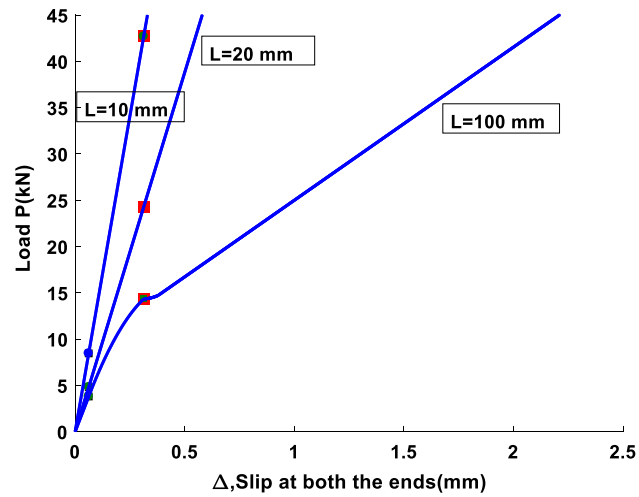

Fig. 15 Interfacial load–displacement curves for various bond lengths

In Fig. 15, the green scatter points represent the elastic stage and red scatter points represent the softening stage. It can be observed from the above figure that the bonding lengths of 10 mm and 20 mm which depict the crack spacing in UHPFRC-strengthened beams take substantial loads to attain the limit of elastic and softening states. But in real conditions, the stresses in the plate at two adjacent cracks in an RC beam are always different; however, this difference may be small. So a value of $\beta < 1$ should be taken and the behaviour should be studied again in the future studies. As of now, the assumption taken for this study is reasonable as no debonding failure was observed for the specimens in between the adjacent cracks of constant bending moment and in fact anywhere else in the beam.

With this knowledge of the debonding behaviour of the strengthened beams under static conditions, the scope of problem has been extended to study the debonding behaviour of the strengthened beams under fatigue loading using the Diab model [17].

The values of non-dimensional parameters used in this model are as follows:

$m_1 = 1.2$, $n_1 = 8.673$, and the values of maximum bond slips are those taken for the previous model.

Figure 16 shows the evolution of the slip with number of cycles for a given loading condition. The maximum slip obtained from this model (3.21 mm) is normalized with respect to the other slip values. It can be observed from the above figure that the rate of debonding is high during the initial number of cycles which is followed by the stable propagation of the debonding. It can be clearly seen from Fig. 16 that the rapid propagation stage is missing. This can be viewed as the failure of the specimen without the debonding of the strips as the debonding slip increasing

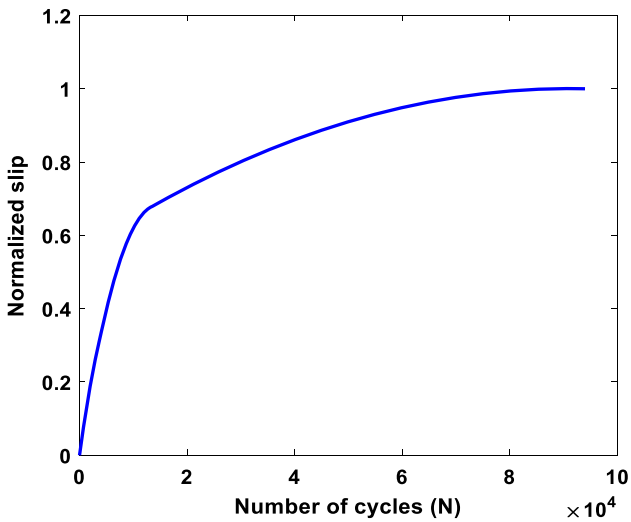

Fig. 16 Normalized slip versus number of cycles

at a stable rate has not grown rapidly in the last few cycles. This can be attributed to the adequate provision of bonding length of the strips.

From the results of the debonding models under both static and fatigue loadings discussed above, it can be inferred that the chances of debonding at the interface of beam–strip is relatively very less in comparison with other materials. Hence, UHPFRC-based strengthening scheme is efficient in making the beam to realize its original strength without any premature failure due to debonding.

Conclusion

Existing analytical models on the debonding behaviour of concrete beams strengthened with composite strips are studied which can be applied to UHPFRC strip-strengthened beams.

1. The bond–slip behaviour of the strips bonded to the concrete substrate at the strip and region between the adjacent cracks in the constant bending moment zone is studied through comprehensive review of the existing models on debonding behaviour.
2. The debonding behaviour of the strips due to the interfacial stresses at the strip end and between the adjacent cracks in the flexure region is studied through debonding models.
3. Debonding of the strips was not observed during the experimental investigations, and the same has been predicted in fair agreement by the analytical models for debonding.

Acknowledgements The authors thank the staff of the Fatigue and Fracture Laboratory and Theoretical and Computational Mechanics Laboratory of CSIR-SERC for the cooperation and suggestions provided during the investigations. This paper is being published with the kind permission of the Director, CSIR-SERC.

Funding Authors acknowledge the funding provided by UGC-UKERI collaborative project between CSIR-Structural Engineering Research Centre and Cardiff University, UK.

References

1. C.K.Y. Leung, Delamination failure in concrete beams retrofitted with a bonded plate. J. Mater. Civ. Eng. **13**(2), 106–113 (2001)
2. W.M. Sebastian, Significance of mid-span debonding failure in FRP-plated RC beams. J. Struct. Eng. **127**(7), 792–798 (2001)
3. P. Wantanasiri, A. Lenwari, Intermediate crack-induced debonding analysis for RC beams strengthened with FRP plates. Struct. Eng. Mech. **56**(3), 473–490 (2015)
4. S.T. Smith, J.G. Teng, Interfacial stresses in plated beams. Eng. Struct. **23**(7), 857–871 (2001)
5. N. Pesic, K. Pilakoutas, Concrete beams with externally bonded flexural FRP-reinforcement: analytical investigation of debonding failure. Compos. Part B Eng. **34**, 327–338 (2003)
6. H.S. Shen, J.G. Teng, J. Yang, Interfacial stresses in beams and slabs bonded with a thin plate. J. Eng. Mech. **127**(4), 399–406 (2001)
7. J.F. Chen, J.G. Teng, Shear capacity of FRP-strengthened RC beams: FRP debonding. Constr. Build. Mater. **17**(1), 27–41 (2003)
8. M. Shahawy, T.E. Beitelman, Static and Fatigue performance of RC beams strengthened with CFRP laminates. J. Struct. Eng. **125**, 613–625 (1999)
9. C.G. Papakonstantinou, P.N. Balaguru, M.F. Petrou, Analysis of reinforced concrete beams strengthened with composites subjected to fatigue loading. ACI Spec. Publ. **206**, 41–60 (2002)
10. Anish, A. Kumar, Ultimate strength analysis of laminated composite sandwich plates. Structure **14**, 95–110 (2018)
11. A. Kumar, A. Chakrabarti, P. Bhargava, V. Prakash, Efficient failure analysis of laminated composites and sandwich cylindrical shells based on higher order zigzag theory. J. Aerosp. Eng. (ASCE) **28**, 1–14 (2015)
12. A. Kumar, A. Chakrabarti, P. Bhargava, R. Chaudhary, Probabilistic failure analysis of laminated sandwich shells based on higher order zigzag theory. J. Sandw. Struct. Mater. **17**, 546–561 (2015)
13. A. Kumar, A. Chakrabarti, Failure analysis of composite skew laminates. Procedia Eng. **173**, 1560–1566 (2017)
14. A.K. Chaubey, A. Kumar, A. Chakrabarti, Novel shear deformation model for moderately thick and deep laminated composite conoidal shell. Mech. Base Des. Struct. Mach. **46**, 650–668 (2018)
15. A. Tounsi, Improved theoretical solution for interfacial stresses in concrete beams strengthened with FRP plate. Int. J. Solids Struct. **43**(14), 4154–4174 (2006)
16. J.G. Teng, H. Yuan, J.F. Chen, FRP-to-concrete interfaces between two adjacent cracks: theoretical model for debonding failure. Int. J. Solids Struct. **43**(14), 5750–5778 (2006)
17. H.M. Diab, Z. Wu, K. Iwashita, Theoretical solution for fatigue debonding growth and fatigue life prediction of FRP-concrete interfaces. Adv. Struct. Eng. **12**, 53–65 (2009)
18. O. Rabinovitch, Y. Frostig, Experiments and analytical comparison of RC beams strengthened with CFRP composites. Compos. Part B Eng. **34**(8), 663–677 (2003)
19. J. Yang, C.F. Chen, J.G. Teng, Interfacial stresses in plated RC beams under arbitrary symmetric load: a higher-order closed form

solution, in Proceedings of the first international conference on the use of advanced composites in construction, Southampton University, pp. 153–163 (2002)
20. F. Yuan, J.G. Teng, R. Seracino, Z.S. Wu, J. Yao, Full-range behaviour of FRP-to-concrete bonded joints. Eng. Struct. **26**, 553–565 (2004)
21. A.R.C. Murthy, M. Aravindan, P. Ganesh, Prediction of flexural behaviour of RC beams strengthened with ultra-high performance fiber reinforced concrete. Struct. Eng. Mech. **65**(3), 315–325 (2018)
22. A.R.C. Murthy, N.R. Iyer, B.K. Raghu Prasad, Characterization and evaluation of micro-mechanical properties of ultra high strength concrete by using micro-indention test. J. Inst. Eng. (India) Ser. A **97**(3), 231–238 (2016)
23. M.A. Carbonell, D.K. Harris, S.V. Shann, T.M. Ahlborn, Bond Strength between UHPC and normal strength concrete (NSC) in accordance with Split prism and freeze & thaw cycling tests, in Proceedings of Hipermat 2012—3rd international symposium on UHPC and nanotechnology for construction materials. Kassel, Germany: Kassel University Press (2012)
24. G. Upreti, A.R.C. Murthy, G. Smitha, N.R. Iyer, L. Venkat, Strength and ductility of RC beams strengthened with ultra high strength cementitious composite overlay. JOSE, Chennai **43**(2), 190–198 (2016)
25. R. Piyasena, Y.C. Loo, S. Fragomeni, Factors influencing spacing and width of cracks in reinforced concrete: new prediction formulae. Adv. Struct. Eng. **7**(1), 49–60 (2004)

Publisher's Note Springer Nature remains neutral with regard to jurisdictional claims in published maps and institutional affiliations.